water

MDPI

Article

Impact Analysis of Karst Reservoir Construction on the Surrounding Environment: A Case Study for the Southwest of China

Huan Shen [1], Yong Huang [1,*], Yuzhou Tang [2], Huiyang Qiu [1] and Ping Wang [1]

[1] School of Earth Science and Engineering, Hohai University, Nanjing 210098, China; shenh@hhu.edu.cn (H.S.); qiuhuiyang@hhu.edu.cn (H.Q.); pingwang@hhu.edu.cn (P.W.)

[2] Jiangsu Academy of Environmental Industry and Technology, Nanjing 210036, China; tangyuzhou2011@gmail.com

* Correspondence: hyong@hhu.edu.cn; Tel.: +86-139-5187-6225

Received: 26 September 2019; Accepted: 5 November 2019; Published: 7 November 2019

Abstract: With the rapid growth of the global demand for low-carbon energy, the development of hydropower has ushered in new development, but the ecological and environmental problems caused by this cannot be ignored. Taking the safe and efficient operation of water conservancy projects as the goal, this paper took the Maling Water Conservancy Project (MWCP) as an example to predict and evaluate the ecological environment risks of water conservancy projects. Based on the on-site geological surveys and experiments, the big well method and the long narrow horizontal tunnel method were used to estimate the water inflow from the underground caverns. The contaminant migration model was used to predict and analyze the groundwater quality. The impact of the MWCP on the surrounding environment was systematically analyzed and evaluated. The results showed that the estimated water inflow from the underground powerhouse and the water conveyance pipeline was about 7403.6 m^3/d during the construction period. The groundwater level in the reservoir area could recover after a short drop, which had little effect on the surrounding vegetation. The groundwater quality was affected obviously because the migration speed of contaminants was very fast under abnormal conditions. During the operation period, it had little effect on groundwater level and had certain influence on groundwater flow field in local area. The source of sewage was mainly a small amount of domestic sewage, which could be ignored after taking anti-seepage measures. After storing water in the reservoir area, there was a possibility of small-scale immersion on the right bank. Most of the reservoirs had good stability conditions but the stability of the upper fault valley was poor; however, the possibility of leakage was very small. Overall, the project had little impact on the surrounding environment. The research results could also provide some references for other hydroelectric projects within the basin.

Keywords: water conservancy project; environmental effects; water inflow; contaminant migration

1. Introduction

Due to the excessive exploitation of traditional energy sources such as coal and oil and the global demand for low-carbon energy, the attention paid to clean energy such as water has increased in recent years. Many countries and cities have built large-scale water conservancy projects within the basin to satisfy social and economic development. The development scale and speed are beyond imagination, especially in certain emerging economies and developing countries [1,2]. The number of large dams in the world has exceeded 50,000 to date (ICOLD 2016). Hydropower is one of the oldest energy sources, an efficient and clean technology that provides about 19% of the world's electricity. It is considered to be

the most sustainable renewable energy after wind power and is playing an important role in drinking water irrigation, flood and drought control, and energy [3]. The world-famous Lancang-Mekong River has a total length of 4909 km, a drainage area of 795,000 km^2 [4], and an average annual flow of 14,500 m^3/s [5]. The Mekong River Dam Database (GMDD) shows that the number of hydropower stations with installed capacity exceeding 15 MW has reached 187, of which 64 are already in use. Furthermore, 18 of those dams in China have a power generation capacity of 17,770 MW and 90% are installed on the upstream dam of Lijiang River [6]. India is the seventh largest hydropower producer in the world with more than 5200 dams in the country. More than 400 are under construction covering the three major river basins of Ganges, Indus, and Yarlung Zangbo, with a total storage capacity of more than 300 billion m^3 [7].

Due to the impact of global climate change and human activities, great changes have taken place in the river and lake system structure on the earth [8–10]. Human activities represented by water conservancy projects among them have the most significant impact on rivers [11]. As an important influence of national economic development and agricultural production, water conservancy projects play an important role in strategic control of water resources and solving the problem of unequal distribution of water resources. On the other hand, artificial interference in the natural state of the river has a significant impact on the surrounding environment, such as frequent geological disasters, change of channel morphology, interruption of fish migration, loss of river habitat, change of water quality, and change of water flow conditions, etc. [12–14].

International experts and scholars have done a lot of theoretical research on the impact of water conservancy projects on the environment so far [15–21]. For example, Hecht et al. [22] established a basin hydrological model for the Mekong River basin and predicted and evaluated the hydrological effects of the upper and lower reaches of the Mekong River on the main stream and tributaries. The research results of Lauri et al. [23] showed that within the coming 20–30 years, the operation of planned hydropower reservoirs is likely to have a larger impact on the Mekong hydrograph than the impacts of climate change, particularly during the dry season. Kobler et al. [24] established a two-dimensional hydrodynamic and water quality coupling based on the water body of a pumped storage power station and predicted the impact of the reservoir operation and climate change on temperature and water quality in multiple scenarios. A multi-level fuzzy relation matrix model was established by Li et al. [25] to comprehensively evaluate the environmental impact of water conservancy hubs. Riyadh et al. [26] and Rossi et al. [27] used the soil and water assessment tool (SWAT) to conduct hydrological impact assessment on the Mekong basin. Vu et al. [28] introduced some globally gridded high-resolution precipitation datasets into SWAT to simulate hydrological influence of reservoir. Robescu et al. [29] introduced the concept of water footprint to analyze and study the environmental and social impact of water conservancy projects. Due to the complexity of the relationship between construction and operation of water conservancy projects and environmental systems, most of the existing research has been conducted on surface water bodies and has not produced enough empirical data on the effects of groundwater flow and water quality [30,31]. Taking the Maling Water Conservancy Project (MWCP) as an example, the purpose of this paper is to analyze and evaluate the impact of the MWCP on the surrounding environment. Firstly, the general situation, hydrogeological conditions, and environmental situation of the MWCP are described. Then, the calculation methods and mathematical model of environmental impact analysis are introduced. Finally, the impact of the MWCP on the surrounding environment is analyzed in detail from multiple perspectives based on the situation of the project area, which provides some references for the construction and operation of a water conservancy project.

2. Study Site

2.1. Study Area

The MWCP is located at the middle reaches of the Mabie River in Xingyi City, Guizhou Province, China, 3 km from the downstream Maling Town, 16 km from Xingyi City, and 318 km from Guiyang

City with very convenient transportation. The reservoir is a karst-gorge type reservoir with a total storage capacity of 128.24 million m^3 and a regulated storage capacity of 107.2 million m^3. The dam height is 90 m and the normal water level of the reservoir is about 1030 m [32]. The engineering tasks are comprehensive utilization of urban and rural water supply, irrigation, and power generation. After the completion, the reservoir provides a 95% guarantee rate of urban water supply and rural domestic water supply, an 80% guarantee rate of irrigation, and a 90% guarantee rate of power station design. The location of study area is shown in Figure 1.

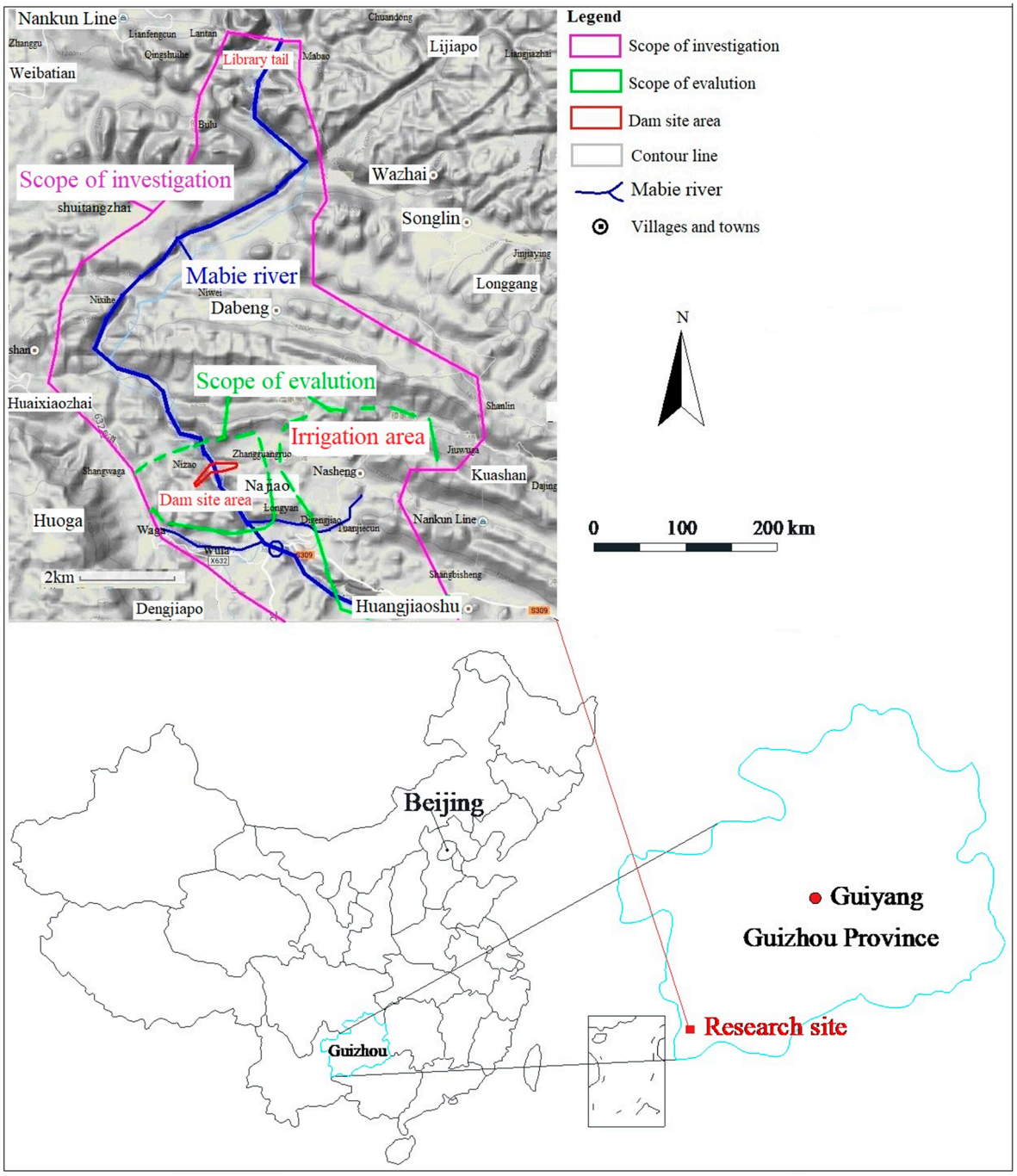

Figure 1. Location of study area.

The study area is located in the southern part of the Yunnan-Guizhou Plateau with low terrain from north to south, which belongs to the slope of the transition from the Yunnan-Guizhou Plateau to the Guangxi Hill. Among them, the northern maximum is about 1600 m and the elevation from the south to the dam site is between 1100 and 1200 m [33]. A layered landform pattern is formed and there are three levels of contour from the watershed to the riverbed because of the large-scale intermittent uplifting movement during the Himalayan period:

(1) The denuded surface of Daloushan stage: The elevation is between 1500 and 1600 m, which was formed in the early Tertiary and found in the watershed area on both sides of the Mabie River. Most of the terrain has been weathered and eroded, only partially retaining the peaks, such as Taichangchong (1581 m), Niutou slope (1500 m), Laoying mountain (1539.6 m), Wutai slope (1555 m), Jiutou mountain (1553 m), and Taishan slope (1643 m) in the north of the area.

(2) The denuded surface of Shanpen stage: The elevation is 600–1100 m, which was formed in the late tertiary period and mainly distributed on the banks of the Mabie River. It is shown as karst landform features such as karst peak cluster depressions, peak forest valleys, and karst gorges, etc.

(3) The denuded surface of Nanpanjiang stage: The earth's crust has been strongly uplifted and the river has been cut down sharply since the fourth period of the first emperor. It is manifested as karst canyon landform. The canyon area is deep from 1100 m to 950 m in the dam area with a depth of 150 m. It formed a "U" or "V" shaped canyon and was mainly developed in the section above Maling. The topography of the MWCP is shown in Figure 2.

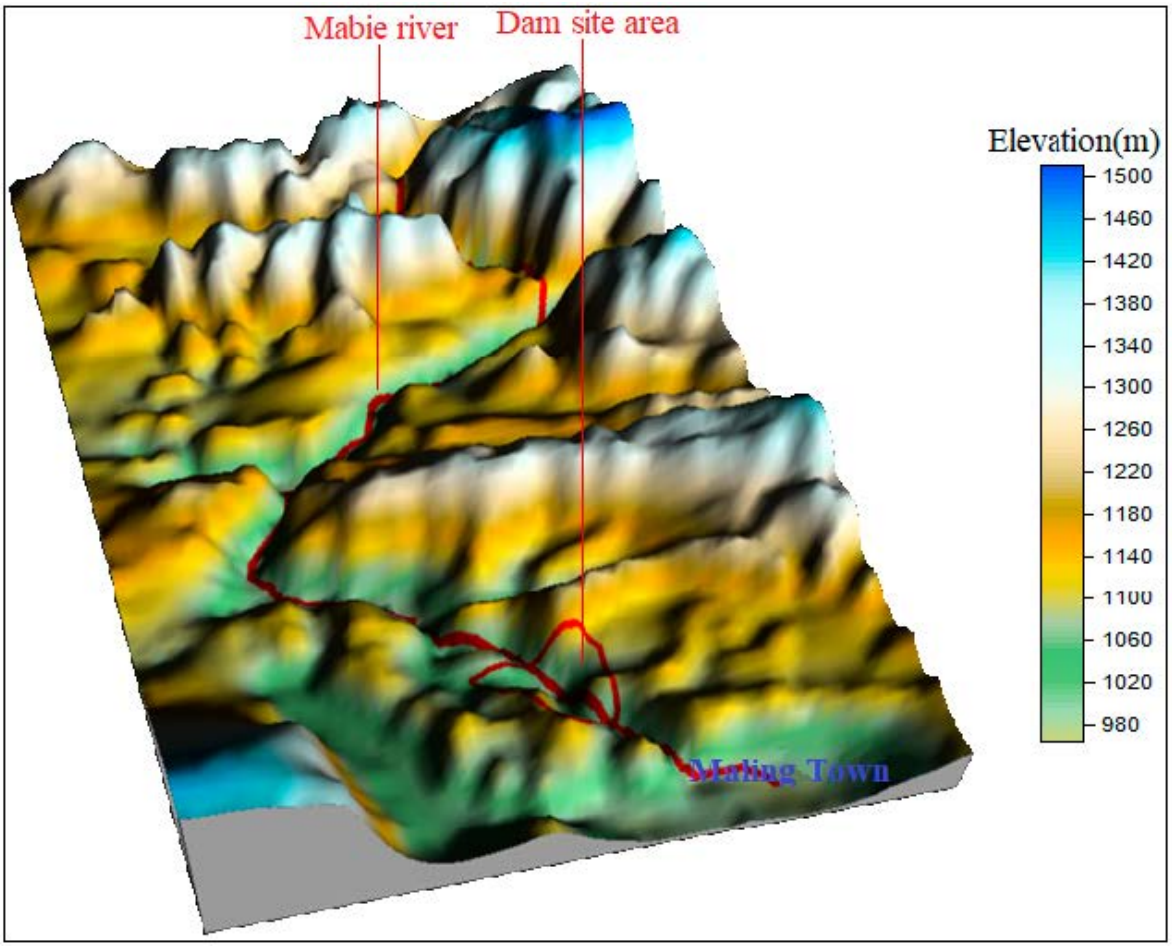

Figure 2. Topography of the Maling Water Conservancy Project (MWCP).

2.2. Meteorological and Hydrological Conditions

The climate of the Mabie River Basin is a subtropical monsoon climate zone with a plateau, monsoon, and warm climate. The climate has vertical differences and the rainfall is quite abundant owing to the disparity in the terrain. There is a meteorological station in the middle reaches of the Mabie River. The distance to the dam site is about 12 km. The elevation of the weather station is 1299.6 m. The average annual temperature is 16.3 °C with the extreme maximum temperature of 36.5 °C (2 May 1994) and the extreme minimum temperature of –4.7 °C (29 December 1983) [34]. The average annual rainfall is 1437.6 mm with the maximum daily value of 244.6 mm. The average annual evaporation is 1512.6 mm (20 cm evaporating dish observation) [35]. The average annual relative humidity is 80% and the minimum relative humidity is close to zero. The average annual wind speed is 2.6 m/s and the maximum wind speed observed in recent years is 13.0 m/s. The maximum snow depth is 1.8 cm (29 December 1983).

The catchment area above the dam site is 1914 km^2. The average annual flow at the dam site is 42.6 m^3/s. The average annual runoff is 1.34 billion m^3 [36]. The annual distribution results of the hydrologic annual runoff in the dam site are shown in Table 1.

Table 1. Statistics of annual flow and runoff in the Maling dam site.

Month	Flow (m^3/s)	Runoff (billion m^3)	Proportion (%)
May	26.00	0.697	5.23
June	95.60	2.480	18.40
July	119.0	3.190	23.70
August	92.00	2.470	18.30
September	63.90	1.660	12.30
October	43.50	1.170	8.75
November	21.40	0.555	4.13
December	12.10	0.324	2.42
January	9.27	0.248	1.86
February	9.02	0.218	1.62
March	8.11	0.217	1.62
April	8.64	0.224	1.67
Total	42.60	13.400	100

2.3. Geological Framework

Permian to Triassic strata and a few tertiary strata are exposed in this area [37,38]. Among them, the T_2g of the Middle Triassic mainly distributes in the reservoir area and most of the engineering area. It is followed by the T_1yn and T_1f of the Lower Triassic, which are exposed in the Nixi River to the Daheishan section. The P_2c and the P_2l of the Upper Permian are exposed in the vicinity of the Nassian anticline to form the core strata of the Nassian anticline. In the east of the Mabie River, it is mostly distributed in the east-west direction, while it is distributed in the northwest–south direction in the west of the Mabie River. The red glutenite of the Tertiary is the clastic rock deposited in a small fault basin. It is only exposed in the Wula and Nahuai area and the minimum exposure elevation is about 950 m. The stratigraphic characteristics of each line are listed in Table 2.

Table 2. Brief description of the regional stratum in the MWCP.

System	Stratum	Thickness (m)	Lithology Brief
Lower Triassic	E_2l	>220	Conglomerate and sandstone.
Triassic	T_2f	>1340	The upper section is a dark gray thin layer sandwiched with thick layer limestone. The lower section is a light-colored thin layer and a medium-thick layer dolomite, dolomitic limestone and collapsible breccia dolomite.
	T_2g	>1200	The upper section is light to dark gray, medium-thick limestone, argillaceous limestone with dolomitic limestone. The lower section is gray-green, yellow-gray, purple-red muddy dolomite, mudstone, and dolomitic limestone.
	T_1yn	>900	Gray-green, purple mud shale, marl, limestone, and dolomite.
	T_1f	500–800	Fuchsia, dark purple sandstone, mud shale, limestone, marl.
Permian	P_2c	2.5–20	Dark gray thick layer of limestone.
	P_21	280	Sandstone sandwiched clay rock and coal seam, bottom bioclastic limestone, limestone.
	P_1m	318–544	Limestone, dolomitic porphyry limestone, argillaceous limestone, siliceous shale.
	P_1q	100	Limestone, argillaceous limestone, dolomitic porphyry limestone and dolomite.

2.4. Hydrogeological Conditions

(1) Groundwater types

According to the nature of aquifers, groundwater flow are divided into three categories: Karst water, fissure water, and pore water, of which karst water is the most important [39].

a. Karst water

The karst water is widely distributed in the study area. It is subdivided into karst pipeline water and karst fissure water. The karst pipeline water mainly exists in the aquifer of the Middle and Upper Cambrian, the Lower Ordovician, the Carboniferous, the Lower Permian, and the Middle and Lower Triassic carbonate section. The water storage space is controlled by karst pipes and caves. The aquifer distribution areas have extremely strong karstification, underground river development, karst springs, caves, sinkholes, and karst depressions, especially in limestone aquifers [40]. There are more than ten karst springs and discharge of each spring is more than 50 L/s. The drilling (well) water flux is between 1000 and 2000 m^3/d and the maximum is about 5000 m^3/d. The runoff modulus of the underground river is between 4 and 7 L/s·km^2. The karst fissure water mainly exists in the aquifer of the Cambrian Quxi Formation, Huaqiao Formation, Carboniferous Yanguan Formation, Permian Wujiaping Formation, Triassic Luolou Formation, Ziyun Formation, and other carbonate rocks and clastic rocks. In this type of aquifer, the water storage space is a dispersion water-conducting structure mainly composed of fissures. The discharge of spring water is 1–10 L/s and the water volume of drilling (well) is generally 500–1000 m^3/d. The amount of individual water can reach 2000–3000 m^3/d. This type of groundwater has a moderate amount of water, but its distribution is more uniform than that of karst pipes.

b. Fissure water

According to the nature of the fractured aquifer, it is further divided into: Clastic rock fissure water, metamorphic rock fissure water, and magmatic rock fissure water. The clastic rock fissure water mainly exists in the clastic rocks of strata of various ages and its water storage space is mainly structural and weathered fissures. Although there are many dew-spring waters in this type of aquifer, the flow rate is not large (less than 5 L/s) and the drilling (well) single-hole water volume ranges from dozens to hundreds m^3/d, dry season groundwater runoff modulus 1–3 L/s·km^2. The metamorphic rock fissure water occurs in metamorphic rock series such as residual sandstone, phyllite, and slate,

etc. Furthermore, the storage space is dominated by weathered fissures. The flow rate of the exposed spring water is generally less than l L/s and the runoff modulus of the groundwater in the dry season is 2–4 L/s·km^2. The magmatic rock fissure water occurs in the basalt, granite, and granitic mixed rock of the Laoshan Mountain and its water storage space is structural fissures and weathered fissures. The flow rate of the exposed aquifers is less than 1 L/s and the runoff modulus of the groundwater is 6–7 L/s·km^2. The water volume is less than 100 m^3/d according to the pumping test in the basalt borehole [41].

c. Pore water

Pore water is sporadically distributed in the pores of the Quaternary and Tertiary unconsolidated loose rock formations. Such aquifers are thin in thickness, small in area, poor in water-containing properties, and small in water volume. The water volume in the borehole is 200–300 m^3/d.

(2) Recharge, runoff, and discharge of groundwater

The main source of groundwater recharge is atmospheric recharge; the river level is higher than the groundwater level in some areas, such as Longdang River, so it is also recharged by the river. Groundwater runoff is mainly in the form of tube and fissure flow. The former is mainly developed in carbonate rock formations and the latter is mostly found in clastic rocks, magma, and metamorphic rocks. They often coexist in the same in a runoff field although they have different properties, and they are closely related to surface water runoff and frequent conversion. There are two main types of groundwater discharge: One is the discharge through the groundwater outlet and the other is the discharge as the form of spring water [39].

2.5. Analysis of Water Intake and Drainage in Engineering

(1) Water intake

The Maling reservoir has seasonal adjustment performance and the annual average water supply will reach 209.82 million m^3 by 2030. The reservoir leakage and evaporation loss is 12 million m^3 and the discharge water volume is 87,700 m^3. The annual average water supply accounted for 15.7% of the average natural runoff of the dam site for many years. The discharge of the reservoir and most of the abandoned water in the water receiving area are still returned to the downstream channel to meet the water function zoning requirements. The initial storage of water from the power station came from surface water, which has little impact on the local groundwater. The overall utilization rate of the Mabie River is about 11.35% and the scale of project water intake is basically reasonable [32].

(2) Drainage

The construction of this project may cause underground water inrush during underground tunnel construction, such as underground powerhouse caverns, water delivery systems, water supply pipelines, and channel excavation, etc. According to the forecast, the underground cavern displacement during the construction period is about 6000–8000 m^3/d, which is between 2000 and 10,000 m^3/d. During the operation of the project, the adjusted water volume is recycled in the upper and lower reservoirs. Although there are karst pipes, the leakage can be effectively controlled and the water loss is small through the treatment of curtain grouting [41].

2.6. Source and Discharge of Sewage

The source of wastewater pollution during the construction period mainly came from the production wastewater generated by the gravel aggregate processing system, concrete processing system, machine repair and maintenance, and the domestic sewage of construction workers, etc. (Table 3).

Table 3. Wastewater discharge statistics of projects during construction period (obtained from MWCP [41]).

Types	Contaminant	Source of Pollution	
		Concentration (mg/L)	Production Amount (m^3/d)
Sand and gravel processing system wastewater	Suspended solids	4.4×10^4	3840.0
Concrete mixing system wastewater	Suspended solids	5000	9.0
Oily wastewater	Suspended solids Petroleums	5000 40	144.0
Foundation pit wastewater	Suspended solids	2000	152.6
Domestic sewage	BOD_5(Biochemical oxygen demand 5) COD(Chemical oxygen demand)	200 400	91.2

In addition to the production wastewater and domestic sewage during the construction of the project and the domestic sewage during the operation period, other sources of pollution in the construction project area were also investigated.

(1) Source of pollution in library tail

The pollution sources above the reservoir of Maling Reservoir include the pollution sources of the main stream of Mabie River and the tributaries of Mulang River. According to the survey, industrial pollution sources mainly come from the Louxia Township of Puan County on the left bank of the Mabie River and the Xinmin Township of Panxian County on the right bank. The emissions of COD, NH_3-N, N, P, Fe, Mn, and Petroleums are, respectively, 8,152,700 kg/a, 408,300 kg/a, 1,823,500 kg/a, 8330 kg/a, 41,000 kg/a, 9830 kg/a, and 36,200 kg/a [41].

(2) Source of pollution in reservoir

Agricultural pollution sources include farmland runoff pollution sources and livestock and poultry breeding sources. According to calculations, the emissions of COD, NH_3-N, N, and P in the Maling reservoir area are, respectively, 5,612,900 kg/a, 683,800 kg/a, 1,504,000 kg/a, and 214,900 kg/a. The source of domestic pollution mainly comes from towns and villages within the reservoir water collection area. According to calculation, the discharge of COD, NH_3-N, N, and P are, respectively, 544,500 kg/a, 114,100 kg/a, 146,200 kg/a, and 12,500 kg/a [41].

2.7. Current Surface and Groundwater Environment

Three underground springs had been monitored by the Environmental Protection Monitoring Station on 19–21 August 2013. The monitoring sections are numbers S1 (Cuizao Village's water well), S2 (spring water point near Maling Town), and S3 (Naxia Village's water well). The monitoring results are shown in Table 4.

Table 4. Groundwater quality monitoring results (mg/L, water temperature (°C), pH is dimensionless) (obtained from MWCP [41]).

Projects	Monitoring Results								
	August 19			August 20			August 21		
Monitoring section	S1	S2	S3	S1	S2	S3	S1	S2	S3
Water temperature	23.0	21.0	22.0	20.4	20.4	21.4	20.5	20.4	21.0
pH	7.14	7.16	7.4	7.12	7.28	7.42	7.15	7.3	7.48
Total hardness	378.4	380.4	272.3	376.4	378.4	274.3	376.4	378.4	274.3
Soluble solid	594	578	412	630	504	446	714	738	486
Permanganate index	1.4	0.7	1.4	0.6	0.9	0.5	0.5	0.8	0.7
NH_3-N	0.70	1.12	0.94	0.74	1.17	1.23	1.06	1.19	1.08
NO_3-N	9.71	14.00	4.23	12.29	14.24	3.91	12.81	14.34	4.07
P	0.02	0.01	0.01	0.01	0.02	0.04	0.01	0.01	0.01
Pb	ND [1]	ND	ND	ND	ND	ND	ND	ND	ND
Cd	0.0001	0.0001	ND	ND	0.0001	0.0002	0.0002	0.0002	ND
Fe	0.07	0.06	0.17	0.08	0.08	0.21	0.07	0.08	0.19

[1] ND means not detected.

3. Methods

3.1. The Big Well Method

The big well method is a method for calculating the inflow of water based on the development of the well theory. In other words, the complex system in the region is equivalent to a large well in operation. The relatively stable groundwater radiation flow field is formed around the well, so the inflow of water is calculated using Dupuit's equation. The underground powerhouse of the MWCP is relatively regular. The top and bottom floors are horizontal and the aquifer is homogeneous. When calculating the water inflow, the entire underground powerhouse is equivalent to a well with a large radius. The method is simpler and more economical than other methods in engineering practice and good results can be obtained. The calculation formula is as follows [42]:

$$Q = 2.73\frac{KMs_w}{\lg\frac{R}{r_w}} \text{ (Confined well)} \quad (1)$$

$$Q = 1.366K\frac{(2H_0 - s_w)s_w}{\lg\frac{R}{r_w}} \text{ (Unconfined well)} \quad (2)$$

$$Q = 1.366\frac{K(2H_0M - M^2 - {h_w}^2)}{\lg\frac{R}{r_w}} \text{ (Confined-unconfined well)} \quad (3)$$

where Q is the water inflow (m^3/d), K is the permeability coefficient (m/d), M is the aquifer thickness (m), s_w is the water level depression (m), R is the influence radius (m), r_w is the large well radius (m), H_0 is the boundary head (m), and h_w is the well water level (m).

3.2. The Long Narrow Horizontal Tunnel Method

The water pipeline of the MWCP was divided into two parts: The water conveyance pipeline of the plant and the water conveyance pipeline of the irrigation zone. According to the results of the on-site drilling pressurized water tests and the weathering characteristics of the rock mass, a weak aquifer with a large thickness exists in a certain extent below the water conveyance pipe. The long narrow horizontal tunnel method is used to calculate the water inrush problem of the tunnel. It is considered that the water pipeline is generalized into a narrow horizontal tunnel, which has the advantages of simplicity, speed, and universality. Furthermore, it is widely used in the construction of hydropower projects and mining engineering. Therefore, the water inflow of pipeline can be calculated

using the non-complete horizontal tunnel of the unconfined water. The formula for calculating the water inflow in a narrow horizontal tunnel is expressed as [43]:

$$Q_1 = \frac{KB}{2}\left[\frac{(H_1-T)^2}{R_1} + \frac{(H_2-T)^2}{R_2} + \frac{2\pi S}{\ln\frac{2T}{\pi b} + \frac{\pi R_1 R_2}{T(R_1+R_2)}}\right] \quad (4)$$

$$Q_2 = \frac{\alpha'(P-E)}{1000\times 30}\times F \quad (5)$$

$$Q = Q_1 + Q_2 \quad (6)$$

where Q_1 is the normal water inflow of the water pipeline (m^3/d), K is the permeability coefficient (m/d), B is the length of the water pipeline (m), H_1 and H_2 are, respectively, the water level at both sides of the water pipeline (m), T is the distance from the bottom of the pipeline to the water-repellent floor (m); R_1 and R_2 are, respectively, the influence widths of the pipeline in the direction of recharge and discharge (m), S is the water level deepening (m), b is the bottom width of the pipe (m), Q_2 is the amount of water inflow when considering the effects of rainfall and evaporation (m^3/d); α' is the effective rainfall infiltration replenishment coefficient, P is the monthly average rainfall (mm), E is the monthly average evaporation (mm), F is the rainfall infiltration recharge area (m^2); and Q is the total influx of the water pipeline (m^3/d).

3.3. Contaminant Migration Model

According to the *Technical Guidelines for Environmental Impact Assessment-Groundwater Environment* (HJ610-2016), the impact of pollutants on groundwater can be predicted by analytical methods for the three-level evaluation project of the reservoir. The supply and discharge of water flow are not considered in the calculation process. Moreover, the adsorption, volatilization, and biochemical reactions of contaminants in the aquifer are not considered and will be considered as conservative pollutants, which can simplify the groundwater flow and water quality model. The main groundwater pollution route of the MWCP is that a small amount of sewage wastewater infiltrates into the underground during the process of production, collection, or treatment, which has no obvious impact on the groundwater flow field in the reservoir area. The impact prediction of groundwater environment for the reservoir area can adopt the one-dimensional stable flow and one-dimensional hydrodynamic dispersion model recommended by Qian et al. [44]. It can be generalized into a one-dimensional semi-infinitely long porous media cylinder with a constant concentration boundary at one end. The one-dimensional continuous contaminant migration prediction equation is expressed as [45]:

$$\frac{C}{C_0} = \frac{1}{2}erfc\left(\frac{x-ut}{2\sqrt{D_L t}}\right) + \frac{1}{2}e^{\frac{ux}{D_L}}erfc\left(\frac{x+ut}{2\sqrt{D_L t}}\right) \quad (7)$$

$$u = K\times I \quad (8)$$

$$D_L = a_L\times u \quad (9)$$

where x is the distance at which the predicted point is from the source (m), t is the predicted time (d), C is the concentration of the contaminant at time t (mg/L), C_0 is the initial concentration (mg/L), u is the water flow velocity (m/d), D_L is the longitudinal diffusion coefficient (m^2/d), *erfc* is the residual error function, K is the permeability coefficient (m/d), I is the hydraulic gradient, and a_L is the longitudinal dispersion. A schematic diagram of the migration of contaminants in a one-dimensional stable flow of hydrodynamic dispersion is shown in Figure 3.

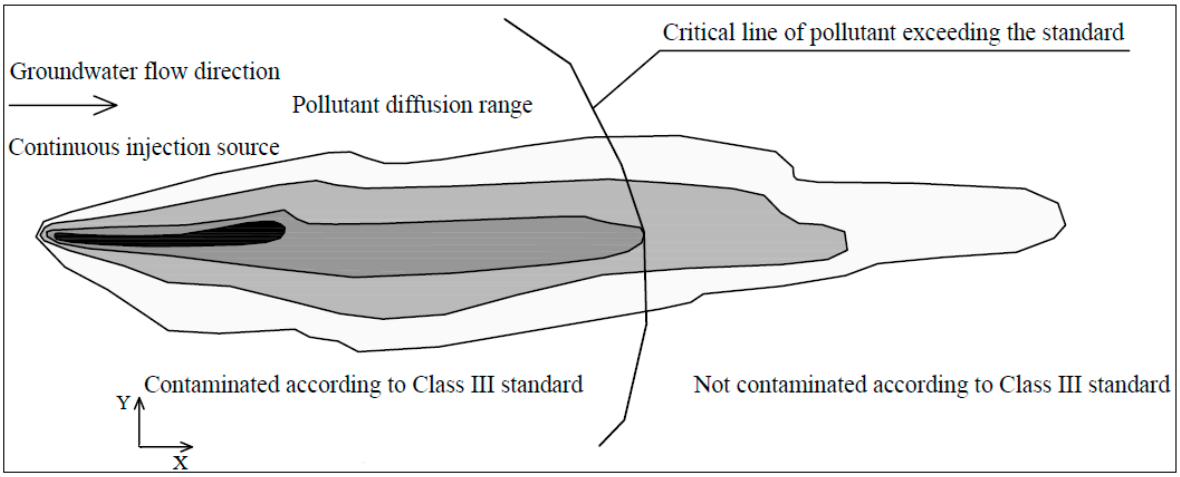

Figure 3. Schematic diagram of contaminant transport.

4. Results Analysis

4.1. Analysis of Spring Water

There are mainly seven springs around the dam site (Figure 4, Table 5). During the construction of the underground cavern, the excavation depth of the water supply system and underground power plant was below the groundwater level. The groundwater level of the plant was about 2–5 m lower than that of the natural conditions. The water pipeline was reduced by 5–20 m. In the area far from underground power plants and right bank water pipelines, groundwater levels had fallen less. The construction had a small effect on the spring water because of the small depth of the left bank water pipeline (about 15–20 m). In addition, the springs in the project area are mainly recharged by atmospheric precipitation and the anti-seepage measures of the caverns started to run after the construction was completed. The spring water flow would be restored because the groundwater volume in the project area was gradually supplemented.

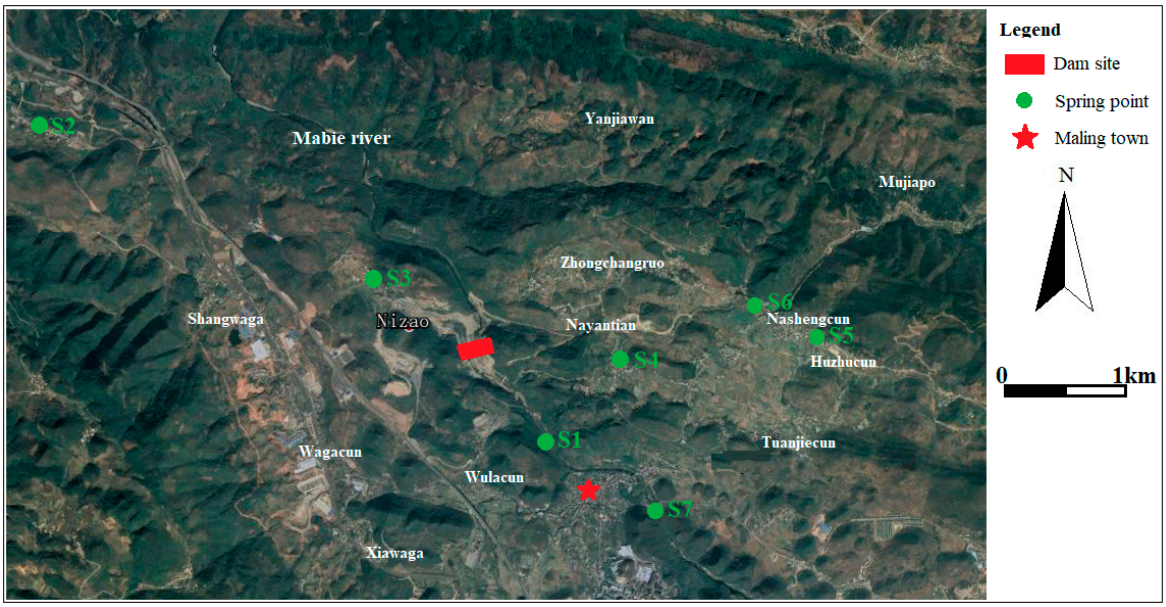

Figure 4. Distribution of karst spring water.

Table 5. Exposure of spring water around the study area.

Distribution Location	Number	Coordinate		Exposed Elevation (m)	Distance from the Dam Site Area (km)	Flow (L/s)	Spring Types
		Longitude	Latitude				
10 m upstream from PM-1	S1	104°54′11.93″	25°11′49.07″	965	0.82	0.2	Descending spring
Nahuai Bridge in Lianfeng Village	S2	104°51′27.06″	25°13′21.46″	1001	4.95	0.5	Descending spring
Nizao Village	S3	104°53′15.43″	25°12′35.05″	1058	1.57	1.5	Descending spring
Next to the Longdang River in Unity Village	S4	104°54′35.02″	25°12′12.54″	1084	1.12	2.0	Descending spring
Huzhu Village	S5	104°55′36.70″	25°12′17.71″	1103	1.71	1.5	Descending spring
Nasheng Village	S6	104°55′18.13″	25°12′28.06″	1202	1.90	0.5	Descending spring
Maling Hydrological Station	S7	104°54′47.00″	25°11′28.11″	959	1.91	5.0	Descending spring

4.2. Analysis of Reservoir Immersion

According to the geological survey of the reservoir area, there was no large-scale immersion (i.e., inundation) problem along the banks of the reservoir area. However, there was a possibility of small-scale immersion in the area around the Nizao village on the right bank of the reservoir. The area was a shale depression of mud shale and dolomite that originates from T_2g^2 and T_2g^{1-2}, with an area of about 0.15 km^2. The farmland was widely distributed on the ground, with a minimum elevation of 1030.6 m. On the east side, there was spring water at the interface between T_2g^2 and T_2g^{1-2} with an elevation of 1042 m. After the reservoir water returned to the mud gully, it was only 200 m away from the lowest point of the depression. The terrain between the two places was gentle and low (the highest point was only 1041.15 m). The lithology was weak and broken, which could not effectively block the penetration of the reservoir water into the depression. Therefore, with the elevation of the water level in the reservoir, the groundwater level in the Nizao village increased correspondingly and resulted in the immersion of farmland in the depression. Meanwhile, the poor drainage of the depression was also likely to cause short-term water logging.

4.3. Stability Analysis of Reservoir Bank Slope

When the reservoir had a normal water storage level of 1030 m, it would return to the 2 km above Longyingzhai. The total length of the backwater was 21 km. The water level varies from 0 to 80 m. The length of the mud shale reservoir section was 3.3 km and the limestone reservoir section was 17.7 km accounting for 16% and 84% of the total length of the reservoir. As the stratigraphic extension extended near the EW direction, most of the valleys became lateral valleys or oblique valleys and only a few river valleys were toward the valley. The slopes of the canyons were composed of bedrock. Both sides of the reservoir had good stability conditions for most of the reservoirs. The stability of the Chahe section and the Nayang section upstream of the dam site was poor due to the development of the slopes and fault valleys.

4.4. Leakage Analysis in the Reservoir Area

(1) Analysis of leakage in adjacent valley

The rock stratum of the dam site intersected with the river at a large angle (50°–60°) and steeply descended downstream. The degree of karst development was controlled by lithology. The karst permeability distribution extended continuously to both sides, while the water permeability along the upper and lower reaches of the river was characterized by interphase distribution. The karst developed weakly because of the distribution of soluble and non-soluble rocks. The mountains on both sides of the reservoir were majestic with high surface and underground watersheds. There were no low neighboring valleys. Although the karst was more developed in the reservoir area, no large pipelines

occurred in the reservoir. Therefore, there was no possibility of karst leakage from the large-scale adjacent valley.

(2) Analysis of leakage between river blocks on the right bank of the reservoir area

At 1.6 to 3.5 km upstream of the dam site, the Mulang River and the Mabie River meet on the right bank of the reservoir. An interstream block was formed between the Mabie River–Mulang River and the Wula river because the reservoir backwatered to the upper part of Mulang river. The narrowest part of the inter-river block was about l km when the normal water level was 1030 m. The stratum is T_1yn limestone, T_2g dolomite, gray dolomite mud shale, and T_1f red sand shale. The red conglomerate strata of E_2l are widely distributed roughly east–west. The faults F_2 and F_3 are also developed along the east–west direction and a small number of unidentified faults cross the stratum in the north–south direction. However, due to the distribution of red sand shale between the Mulang River and the Wula River with a thickness of 625 m, which blocks the hydraulic connection between the Mulang River and the Wula River, the possibility of leakage is very small (Figure 5a).

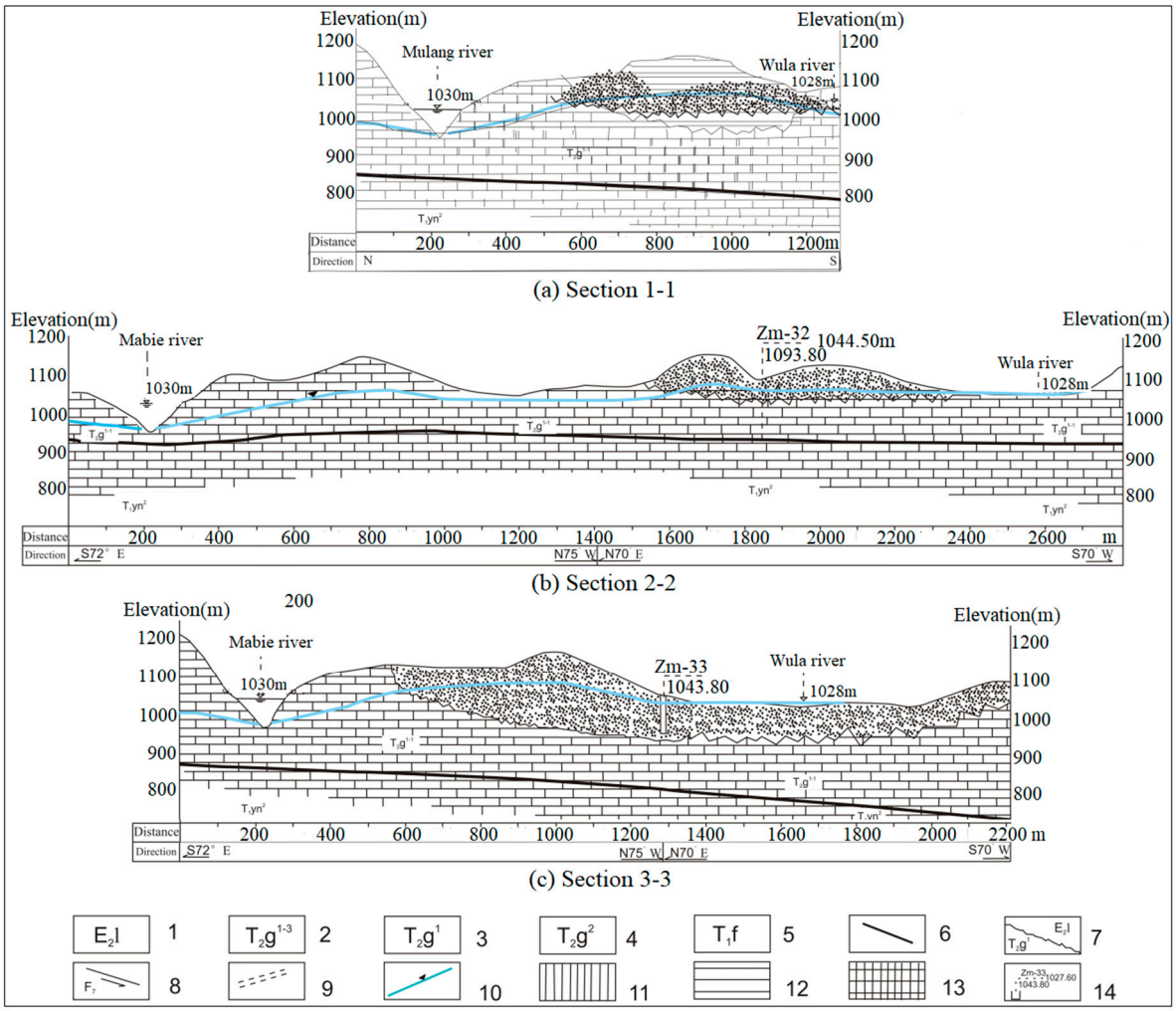

Figure 5. Karst hydrogeological sections of reservoir area.1. Tertiary, fuchsia siltstone, breccia, 2. The lower part of the limestone and dolomite in the lower part of the Guanling Formation, 3. The thin layer to medium thick layer of limestone in the lower part of Yongning Town Group, 4. Thick layer to medium-thick layer limestone in the lower part of Yongning Town, 5. Feixianguan Formation siltstone and mud shale, 6. Composite formation boundaries, 7. Unconsolidated stratigraphic boundaries, 8. Faults and numbers, 9. Speculated karst pipeline, 10. Groundwater level line, 11. A fractured aquifer, 12. Karst aquifer, 13. Relative to the water barrier, 14. Drill number (upper number), elevation (lower number) and water level (number on the right).

The Wula River on the right bank of the reservoir originates from the vicinity of Shangwa and is formed by the Daoban Creek and some nearby springs and gullies. It extends east–west in the upper section of Shangwaga. It flows to the south and east in the lower section of Shangwaga. It constitutes a low neighboring valley because its river level is slightly lower than the normal water level of the MWCP (1030 m). The E_2l layer of the inter-river block has good water-blocking performance with small depression in a local area. In addition, the percolation diameter is long (1.2–2 km). The water head inside and outside the reservoir is only 5–10 m and an underground watershed is above the normal water level. Therefore, there is no possibility of leakage along the two layers of T_2g^{1-1} and T_1yn^1. The remaining formations such as T_1yn^2 and T_2g^{1-2} are water-repellent layers and will not leak (Figure 5b,c).

4.5. Analysis of Water Inflow in Underground Caverns

The analysis of water inflow during construction period mainly considered that the excavation of the plant, water diversion system, and left bank irrigation water supply system had not been lined and the anti-seepage drainage system of the plant had not been arranged. At the same time, the outer surface of the plant and the water diversion pipe were treated as the boundary of the escape surface. The upper flat section of the water conveyance system, the location of the tail water tunnel, and the water supply pipeline of some irrigation areas were buried deeper than the groundwater level. The amount of water in the construction was small, so it was not considered. The calculated water inflow in the plant area was 4487.2 m^3/d by the big well method. The calculated water inflow from the water conveyance pipeline was 2916.4 m^3/d by the narrow long horizontal tunnel method.

4.6. Analysis of Groundwater Level

Before the excavation of the water conveyance tunnel and underground powerhouse, the inclined and lower flat sections and the workshop were below the groundwater level (about 990 m) except for the upper flat section of the water conveyance system. The contour map of the groundwater level in different sections during the construction period is shown in Figure 6. The groundwater level plummeted after the excavation of the cavern. The groundwater level descended along the inclined well and it was adjacent to the outer wall of the high-pressure branch pipe, indicating that the unlined diversion well and the high-pressure branch pipe had strong water guiding effect. The decline of the free surface was mainly due to the fact that most of the permeate water flows into the diversion pipe. Finally, a plant-centered landing funnel was formed. Since the floor of the plant was basically the same as the water level of the Mabie River, the groundwater entering the plant through the river was less.

The bottom surface of the plant and the surrounding wall were surrounded by free surfaces, which indicates that groundwater near the plant escapes through the unlined plant floor and the surrounding side walls. The top of the plant was in an unsaturated zone, so no groundwater penetrates into the plant through the top of the plant. The inclined section, the lower section, and the irrigation section of the diversion power generation system were located below the groundwater level line. The construction excavation would cause the groundwater level to drop to a certain extent. The corresponding groundwater anti-seepage measures were taken during the construction of the project. The various measures began to function after the completion of the construction. The surrounding groundwater could quickly return to the natural condition under the effect of the surrounding groundwater, surface water, and rainfall.

After the reservoir was filled with water, the groundwater was mainly discharged from the upper reservoir to the downstream of the dam and the factory building. The water level around the inundation area was relatively high and gradually decreased radially to the surrounding area. The groundwater level in the reservoir tailwater was relatively low. The groundwater level decreased slowly and had little difference with the natural state. The groundwater level of the plant had dropped by about 2–5 m owing to the drainage. The water level of the water pipeline had increased by 10–20 m. The water level of the mountain on both sides had increased by about 15–25 m. The construction had

changed the local seepage field distribution around the underground powerhouse, but the scope of influence was mainly limited to a small area near the plant. Generally speaking, it had little effect on the groundwater level and flow field in the study area after the project operation. However, it had some influence on the groundwater flow field of local areas due to the effect of engineering anti-seepage and precipitation measures, such as the plant.

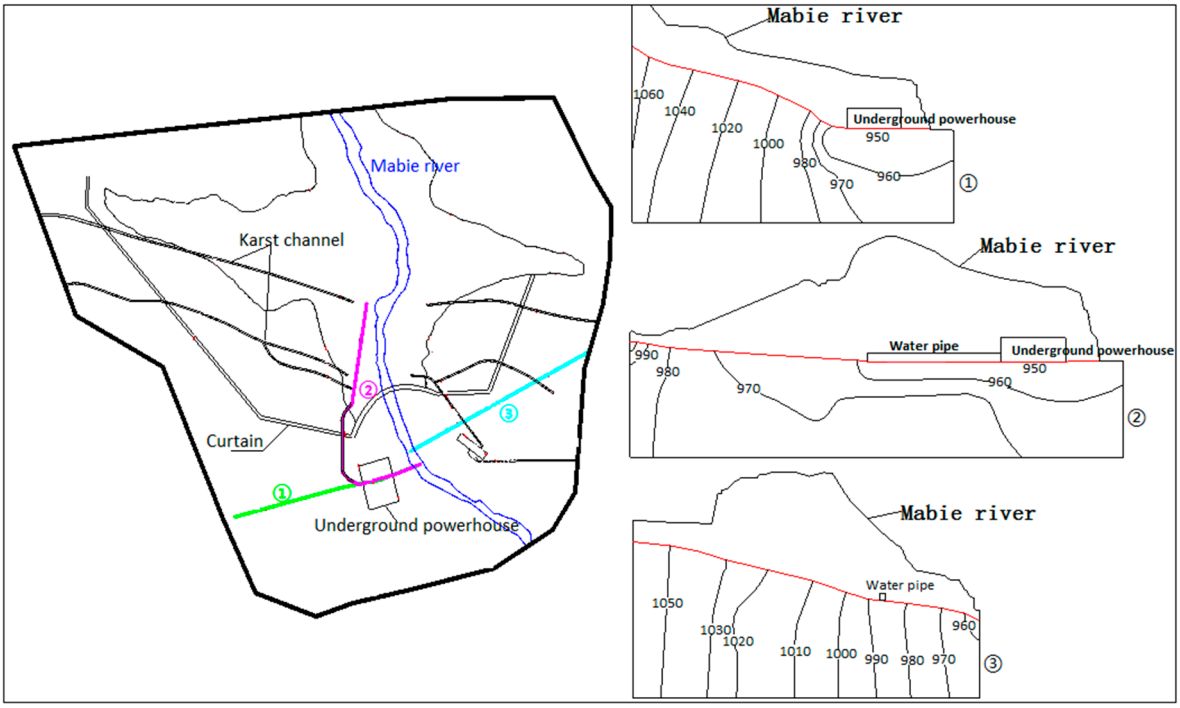

Figure 6. Groundwater level contour map of different sections during construction period.

4.7. Analysis of Groundwater Quality

The main sources of water pollution during construction were gravel processing system wastewater, concrete mixing system wastewater, mechanical repair plant oily wastewater, and foundation pit wastewater. The main contaminants in sewage wastewater were BOD_5, COD, SS, and petroleum. Their concentrations were, respectively, 200 mg/L, 400 mg/L, 5000 mg/L, and 40 mg/L.

(1) Analysis of the impact on shallow groundwater

The engineering exploration data show that the single layer thickness of the first rock layer is Mb > 1.0 m. The permeability of the shallow rock mass is mainly 5–10 Lu (1 Lu is about 10^{-5} cm/s). The vertical permeability coefficient is between 10^{-6}cm/s and 10^{-4}cm/s. The anti-fouling performance of the vadose zone is medium, indicating that shallow groundwater is not susceptible to pollution. If the wastewater is leaking, the contaminants will pass through the aeration zone slowly, which has less impact on the quality of the shallow groundwater.

(2) Analysis of the impact on deep groundwater

Deep groundwater in the project area includes fissure water and karst water according to the analysis of geological conditions. Taking atmospheric precipitation as the main source of recharge, surface water and ditch water are also sources of replenishment of low-altitude karst water and they are excreted in the form of spring water. In summary, there is a certain relationship between regional groundwater aquifers. However, it has little impact on the quality of deep groundwater.

(3) Analysis of the influence of groundwater around the cavern

The project adopted the method of draining or collecting wells and collecting water from the pump and drained the water from the tunnels. Finally, it entered the sedimentation tank set up

at the cave and was used for watering, forest irrigation, etc. Therefore, it had little impact on the surrounding groundwater.

The wastewater will leak when the anti-seepage of the wastewater treatment facility is not in place or fails. The leakage during the construction period is about 211.8 m^3/d when the leakage of the sewage is calculated according to 5% of the generated amount. At this time, we could formulate according to Equation (7) to predict the migration of contaminants. The calculation parameters are shown in Table 6. For the contaminants in abnormal conditions, the excess diffusion distance of contaminants after 100 days, 1 year, 3 years, 5 years, and 10 years after the continuous discharge of the wastewater was calculated (Table 7). Under abnormal conditions, the migration distance of contaminants exceeds the standard as the time increases. It shows that if the groundwater is polluted in the karst area, the migration distance of the contaminants is large and the contaminants are easy to spread.

Table 6. Statistical table of calculation parameters.

K [1] (m/d)	I[2]	a_L [3] (m)	u [4] (m/d)	D_L [5] (m^2/d)	C_0 [6] (mg/L)	
					Permanganate Index	Petroleums
0.49	0.1831	70	0.0897	6.279	150	40

[1] K is the permeability coefficient, [2] I is the hydraulic gradient, [3] a_L is the longitudinal dispersion, [4] u is the water flow speed, [5] D_L is the longitudinal diffusion coefficient, [6] C_0 is the concentration of contaminants.

Table 7. Results of prediction of excessive diffusion distance under abnormal conditions (m).

Type of Contaminant	Class III Standard Value (mg/L)	After 100 Days	After 1 Year	After 3 Years	After 5 Years	After 10 Years
Permanganate index	3.00	90.38	186.78	361.78	501.59	800.25
Petroleum	0.05	122.74	249.11	470.88	643.24	1002.15

The source of sewage in the operation period of the reservoir was mainly domestic sewage, which was estimated to be 30 m^3/d. If the anti-seepage measures are in place, the amount of sewage infiltration can be neglected and the operation period of the reservoir has little impact on groundwater quality.

5. Discussion

Based on past data, most water conservancy projects will have problems with reservoir immersion after filling [46]. The MWCP will flood the cultivated land in the reservoir area and promote the change of land use type based on the on-site hydrogeological survey data. During the construction and operation of the project, the increase or decrease of the water level of the river will inevitably pose a threat to the slope stability of the banks on both sides [47]. Most of the reservoirs in Maling have good stability conditions. The stability of the Chahe section and the Nayang section upstream of the dam site is poor due to the development of the slopes and fault valleys. Although the reservoir area is located in the typical karst area of southern China, no large karst pipelines lead to the outside of the reservoir. There are high surface and underground watersheds between the valleys and the possibility of leakage in the reservoir area is eliminated. Potential flow changes from various operations and development scenarios in the Mekong River Basin were presented and discussed from the research results of Piman et al. [48]. In this paper, we considered the two scenarios of construction period and operation period when considering the influence of MWCP on the flow, water level, and water quality in the reservoir area.

The analysis of water inflow during construction period mainly considered that the excavation of the plant, water diversion system, and left bank irrigation water supply system had not been lined and the anti-seepage drainage system of the plant had not been arranged. At the same time, the outer surface of the plant and the water diversion pipe were treated as the boundary of the escape surface according to the relevant research results of the prediction method of the inflow of underground

caverns by Marinelli et al. [49]. The big well method and narrow horizontal tunnel method were used to estimate the water inflow of the underground powerhouse and the water conveyance pipeline, respectively. The estimated water inflow during the construction period was about 6000–8000 m^3/d, which was in good agreement with the engineering practice. The water level after construction excavation had plummeted. The water level of the plant had dropped by about 2–5 m compared with the natural conditions. A falling funnel centered on the underground powerhouse was formed. During the construction process, there were seepage and dripping phenomena along the fractures and karst, which caused short-term water inrush in some areas. The water seepage gradually decreased with time and tended to be stable. The water level in the water pipeline dropped by 5–20 m and the groundwater level in other areas decreased less. Some springs might be affected to some extent and the impact on the upper and surrounding vegetation was small. The main sources of water pollution during construction were gravel processing system wastewater, concrete mixing system wastewater, mechanical repair plant oily wastewater, foundation pit wastewater, and domestic sewage. A small amount of sewage from them infiltrated into the ground and caused groundwater pollution. The effect on groundwater quality under normal conditions was small. Under abnormal conditions where the wastewater treatment facility was impervious to seepage or impervious to failure, it was simplified into one-dimensional stable flow and a one-dimensional hydrodynamic dispersion problem in order to facilitate the construction and calculation of the model. The one-dimensional continuous contaminants transport prediction equation was used to predict the migration of contaminants in groundwater [50]. The maximum distance of contaminants moving along the direction of water flow was about 122.74 m under 100 days of abnormal conditions. The migration speed was very fast and it was necessary to consider the relevant recommendations of Foster et al. [51] for groundwater environmental protection. Construction production facilities and living areas cannot be directly located in limestone, dolomite distribution areas, and where karst pipelines may exist. Production areas and living areas should be filled with clay and concrete. Some anti-seepage measures should be taken to prevent the formation of a continuous source of pollution and minimize the impact on surrounding groundwater.

The corresponding anti-seepage measures for buildings under the operation period had been implemented and gradually began to function, such as water delivery systems, underground power plants, and irrigation water supply pipelines. The leakage of the water pipeline was small, and the leakage of the plant was estimated to be about 1000–3000 m^3/d when the anti-seepage of the curtain was normal. The water level of the underground powerhouse dropped by about 2–5 m because of the engineering seepage and drainage. The water level of the water pipeline increased by 10–20 m and the water level of the mountain on both sides increased by about 15–25 m. The groundwater flow trend in the dam site was concentrated from the upstream of the dam to the downstream and underground powerhouse areas. The water level around the submerged area was relatively high and gradually decreased radially toward the surrounding area. The source of water pollution during the operation period were mainly domestic sewage and oily sewage generated during reservoir maintenance and accidents, accompanied by the production of about 30 m^3/d. The amount of sewage infiltration would be neglected if the anti-seepage measures were in place. Therefore, the reservoir operation period had little impact on groundwater quality.

In summary, our calculation and analysis results showed that the MWCP had a weak impact on the surrounding environment during construction and operation. However, it should be noted that the weak effect is irreversible. Today, hydropower projects are welcoming new developments with the rapid growth of low-carbon energy demand in the world. At the same time as large-scale construction and operation of hydropower projects, more attention must be paid to the impact on the surrounding environment while paying attention to power generation, water storage, and irrigation rates.

6. Conclusions

Some disputes about the advantages and disadvantages of water conservancy projects have not been resolved even as the water conservancy project has received renewed attention. We still need

to pay attention to the impact on the ecological environment while we are building large-scale water conservancy projects for economic and social development. Based on the example of the MWCP in Xingyi City, Guizhou Province, we analyzed the impact on the surrounding ecological environment during the construction and operation phases by using the big well method and other methods. The results of the calculation and analysis were as follows:

(1) There was no large-scale immersion problem along the river banks of the reservoir area. Only in the area around the mud stove village on the right bank of the reservoir was there a possibility of small-scale immersion. Most of the reservoirs in Maling had good stability conditions. The stability of the Chahe section and the Nayang section upstream of the dam site was poor due to the development of the slopes and fault valleys. There were no large karst pipes in the reservoir area leading to the outside of the reservoir. Meanwhile, there were high surface and underground watersheds between the valleys. The possibility of leakage in the reservoir area was small. In the process of hydropower development within the basin, special attention should be paid to the development of karst in the basin to avoid damage to the surrounding environment and dam safety.

(2) During the construction period, the underground water supply and water pipeline had been expected to have a water inflow of about 6000–8000 m^3/d. The groundwater level would drop briefly and a falling funnel centered on the underground powerhouse was formed, which would cause water inrush. With that, the groundwater level would be restored under the effect of surrounding groundwater, surface water, and rainfall, which had little impact on the springs and surrounding vegetation. The maximum distance of contaminants moving along the direction of water flow was about 122.74 m after 100 days under abnormal conditions. It showed that once the groundwater was polluted, the contaminants were easy to spread and the migration speed was very fast, which caused the groundwater quality to be affected. Therefore, it was necessary to pay attention to the impact on groundwater quality when constructing water conservancy projects in karst areas. Protection should be based on prevention and sewage treatment facilities should be regularly inspected (monitoring frequency was less than 100 days). Timely measures should be taken to reduce and eliminate dripping, such as blocking leaking pipes and installing cut-off walls, so as to minimize the impact on surrounding groundwater.

(3) During the operation period, the leakage of the underground powerhouse had been estimated to be about 1000–3000 m^3/d and the leakage of the water delivery pipeline was negligible when the curtain anti-seepage was normal. It had a certain influence on the groundwater flow field in local areas due to the effect of engineering anti-seepage and precipitation measures. However, the scope of influence was mainly limited to a small area near the underground powerhouse. The source of sewage was mainly domestic sewage with a small amount of water, which could be ignored after taking anti-seepage measures. However, a certain number of tracking and monitoring points needed to be set up and emergency disposal measures and plans should be formulated.

Overall, the MWCP in the karst area of southwestern China had little impact on the surrounding environment. Computational analysis methods and conclusions could provide a reference for water conservancy projects in karst areas. In addition, due to the different geological conditions, climatic conditions, and economic development conditions of each water conservancy project and the complexity of the relationship between water conservancy project and the surrounding environment, our research results were limited and preliminary. Further research is needed to assess the impact of hydropower development on irrigation, river sediment flows, and downstream ecosystems.

Author Contributions: H.S. and Y.H. conceived and designed the research theme; Y.H. designed the analytical methods; H.Q. and P.W. contributed to the field investigation and data collection; H.S. and Y.T. analyzed the data; H.S. wrote the paper and Y.H. revised the paper.

Funding: This study was financially supported by The National Natural Science Foundation of China (Grant no. 41572209), and sponsored by a Qing Lan Project of Jiangsu Province (2016B16073).

Conflicts of Interest: The authors declare no conflict of interest.

References

1. Zeng, R.J.; Cai, X.M.; Ringler, C.; Zhu, T.J. Hydropower versus irrigation-an analysis of global patterns. *Environ. Res. Lett.* **2017**, *12*, 034006. [CrossRef]
2. Zhang, X.; Li, H.Y.; Deng, Z.D.; Ringler, C.; Gao, Y.; Hejazi, M.I.; Leung, R. Impacts of climate change, policy and Water-Energy-Food nexus on hydropower development. *Renew. Energy* **2018**, *116*, 827–834. [CrossRef]
3. Auestad, I.; Nilsen, Y.; Rydgren, K. Environmental restoration in hydropower development-lessons from norway. *Sustainability* **2018**, *10*, 3358. [CrossRef]
4. Wang, W.; Lu, H.; Leung, L.R.; Li, H.; Zhao, J.; Tian, F.; Yang, K.; Sothea, K. Dam construction in Lancang-Mekong River Basin could mitigate future flood risk from warming-induced intensified rainfall. *Geophys. Res. Lett.* **2017**, *44*, 10378–10386. [CrossRef]
5. Liu, S.; Lu, P.; Liu, D.; Jin, P.; Wang, W. Pinpointing source and measuring the lengths of the principal rivers of the world. *Int. J. Digit. Earth* **2009**, *2*, 80–87. [CrossRef]
6. Water, Land, and Ecosystems-Mekong. Mekong Hydropower Map and Portal. Available online: https://wle-mekong.cgiar.org/maps/ (accessed on 20 July 2019).
7. Ali, S.A.; Aadhar, S.; Shah, H.L. Projected Increase in Hydropower Production in India under Climate Change. *Sci. Rep.* **2018**, *8*, 12450. [CrossRef]
8. Deng, X.J.; Xu, Y.P.; Han, L.F.; Song, S.; Xue, G.L.; Xiang, J. Spatial-temporal changes in the longitudinal functional connectivity of river systems in the Taihu Plain, China. *J. Hydrol.* **2018**, *566*, 846–859. [CrossRef]
9. Ye, X.C.; Zhang, Q.; Liu, J.; Li, X.H.; Xu, C.Y. Distinguishing the relative impacts of climate change and human activities on variation of streamflow in the Poyang Lake catchment, China. *J. Hydrol.* **2013**, *494*, 83–95. [CrossRef]
10. Dai, X.Y.; Zhou, Y.Q.; Ma, W.C.; Zhou, L.G. Influence of spatial variation in land-use patterns and topography on water quality of the rivers inflowing to Fuxian Lake, a large deep lake in the plateau of southwestern China. *Ecol. Eng.* **2017**, *99*, 417–428. [CrossRef]
11. Shao, W.W.; Chen, X.D.; Zhou, Z.H.; Liu, J.H.; Yan, Z.Q.; Chen, S.L.; Wang, J.H. Analysis of river runoff in the Poyang Lake Basin of China: Long-term changes and influencing factors. *Hydrol. Sci. J.* **2017**, *62*, 575–587. [CrossRef]
12. Liu, J.G.; Zang, C.F.; Tian, S.Y.; Liu, J.G.; Yang, H.; Jia, S.F.; You, L.Z.; Liu, B.; Zhang, M. Water conservancy projects in China: Achievements, challenges and way forward. *Glob. Environ. Chang.* **2013**, *23*, 633–643. [CrossRef]
13. Lu, Y.J.; Yan, D.H.; Qin, T.L.; Song, Y.F.; Weng, B.S.; Yuan, Y.; Dong, G.Q. Assessment of Drought Evolution Characteristics and Drought Coping Ability of Water Conservancy Projects in Huang-Huai-Hai River Basin, China. *Water* **2016**, *8*, 378. [CrossRef]
14. Dong, J.W.; Xia, X.H.; Liu, Z.X.; Zhang, X.T.; Chen, Q.W. Variations in concentrations and bioavailability of heavy metals in rivers during sediment suspension-deposition event induced by dams: Insights from sediment regulation of the Xiaolangdi Reservoir in the Yellow River. *J. Soil. Sediments* **2019**, *19*, 403–414. [CrossRef]
15. Lu, S.L.; Wu, B.F.; Wang, H.; Ouyang, N.L.; Guo, S.Y. Hydro-ecological impact of water conservancy projects in the Haihe River Basin. *Acta Oecol.* **2012**, *44*, 67–74. [CrossRef]
16. Boelens, R.; Shah, E.; Bruins, B. Contested Knowledges: Large Dams and Mega-Hydraulic Development. *Water* **2019**, *3*, 416. [CrossRef]
17. Lyu, Y.W.; Zheng, S.; Tan, G.M. Effects of Three Gorges Dam operation on spatial distribution and evolution of channel thalweg in the Yichang-Chenglingji Reach of the Middle Yangtze River, China. *J. Hydrol.* **2018**, *565*, 429–442. [CrossRef]
18. Ivan, G.M.; Alvaro, S.W.; Luis, G. Hydrological Risk Analysis of Dams: The Influence of Initial Reservoir Level Conditions. *Water* **2019**, *11*, 461.
19. Xiao, X.; Chen, X.H.; Zhang, L.L. Impacts of small cascaded hydropower plants on river discharge in a basin in Southern China. *Hydrol. Process.* **2019**, *33*, 1420–1433. [CrossRef]
20. Le, T.B.; Al-Juaidi, F.H.; Sharif, H. Hydrologic Simulations Driven by Satellite Rainfall to Study the Hydroelectric Development Impacts on River Flow. *Water* **2014**, *6*, 3631–3651. [CrossRef]
21. Sun, D.P.; Lu, R.L.; Song, Y.J.; Yan, J. Impact of hydroelectric projects on river environment: Analysis of water quality changes in Ningxia Reach of Yellow River. *Water Sci. Eng.* **2008**, *1*, 66–75.

22. Hecht, J.S.; Lacombe, G.; Arias, M.E. Hydropower dams of the Mekong River basin: A review of their hydrological impacts. *J. Hydrol.* **2019**, *568*, 285–300. [CrossRef]
23. Lauri, H.; de Moel, H.; Ward, P.J.; Rasanen, T.A.; Keskinen, M.; Kummu, M. Future changes in Mekong River hydrology: Impact of climate change and reservoir operation on discharge. *Hydrol. Earth Syst. Sci.* **2012**, *16*, 4603–4619. [CrossRef]
24. Kobler, U.G.; Wuest, A.; Schmid, M. Combined effects of pumped-storage operation and climate change on thermal structure and water quality. *Clim. Chang.* **2019**, *152*, 413–429. [CrossRef]
25. Li, M.J.; Wu, X.Y.; Jiao, J.G.; Sun, Z.L. Multi-level fuzzy comprehensive evaluation on environmental impact from water control project. *Water Resour. Hydrop. Eng.* **2018**, *49*, 106–110.
26. Riyadh, A.S. SWAT model for Integrated River Basin Management withapplication to the Mekong basin. Symposium on Sediment Dynamics and the Hydromorphology of Fluvial Systems, Dundee, Scotland, July 02–07, 2006. *IAHS Publ.* **2006**, *306*, 601–610.
27. Rossi, C.G.; Srinivasan, R.; Jirayoot, K.; Le Duc, T.; Souvannabouth, P.; Binh, N.; Gassman, P.W. Hydrologic evaluation of the lower mekong river basin with the soil and water assessment tool model. *Int. Agric. Eng. J.* **2009**, *18*, 1–13.
28. Vu, M.T.; Raghavan, S.V.; Liong, S.Y. SWAT use of gridded observations for simulating runoff—A Vietnam river basin study. *Hydrol. Earth Syst. Sci.* **2012**, *16*, 2801–2811. [CrossRef]
29. Robescu, L.D.; Bondrea, D.A. The water footprint from hydroelectricity: A case study for a hydropower plant in Romania. In Proceedings of the Conference on Sustainable Solutions for Energy and Environment (EENVIRO), E3S Web of Conferences, Cluj Napoca, Romania, 9–13 October 2018; Volume 85, p. 06012.
30. Djuma, H.; Bruggeman, A.; Camera, C. The Impact of a Check Dam on Groundwater Recharge and Sedimentation in an Ephemeral Stream. *Water* **2017**, *9*, 813. [CrossRef]
31. Zhang, X. Study on the Characteristics of Groundwater System and Groundwater Environmental Impact at the Left Dam of Wudongde Hydropower Station. Master's Thesis, Chengdu University of Technology, Chengdu, China, 1 May 2015.
32. Guizhou Province Water Conservancy Construction Field Project Information Disclosure Column. Available online: http://xmgg.gzsljg.com/Home/ProjectInfo/59 (accessed on 17 October 2019).
33. Wu, L.N. Study on Temporal and Spatial Distribution of Extreme Precipitation in Typical Geomorphological Areas of Yunnan-Guizhou Plateau Based On GIS. Master's Thesis, Guizhou University, Guiyang, China, June 2018.
34. Guizhou Meteorological Bureau. Available online: http://gz.cma.gov.cn/ (accessed on 17 October 2019).
35. Water Resources Department of Guizhou Province. Available online: http://mwr.guizhou.gov.cn/slgb/slgb1/201811/t20181121_3300137.html (accessed on 17 October 2019).
36. Jiang, Q.F. Study on the Configuration of Diversion and Flood Discharge Structure of Maling Hydropower Project. Master's Thesis, Northwest A & F University, Yangling, China, May 2017.
37. Zhou, T.M. Study on the stratigraphic characteristics and the correlation and division of early—Middle Permian strata in eastern Yunnan, southwestern Guizhou and northwestern Guangxi. *Yunnan Geol.* **1984**, *4*, 367–374.
38. Xiao, J.F.; Wei, J.Y.; Hu, R.Z. The Middy Late Triassic Sequence Stratigraphic Framework in Southwestern Guizhou and Adjacent Regions. *Acta Geol. Sin.* **2004**, *5*, 591–599.
39. Hong, Y.S.; Li, Q.; Yi, S.Y. Groundwater Prospecting Method for the Interstream Block in Deep Valley, Karst Mountain Area. *Acta Geol. Sichuan* **2018**, *38*, 644–647.
40. Zheng, M.Y.; Tang, Y.J. Study on the spatial relationship between karst groundwater system and geological conditions in Baiyunyan area of Guizhou province. *Ground Water* **2018**, *40*, 16–18.
41. *Environmental Impact Report of Maling Water Control Project (MWCP)*; Guiyang Engineering Corporation Limited of China Power Construction Corporation: Guizhou, China, 2015.
42. Zhang, K.; Cao, B.; Lin, G. Using Multiple Methods to Predict Mine Water Inflow in the Pingdingshan No.10 Coal Mine, China. *Mine Water Environ.* **2017**, *36*, 154–160. [CrossRef]
43. Jin, X.G.; Li, Y.Y.; Luo, Y.J. Prediction of city tunnel water inflow and its influence on overlain lakes in karst valley. *Environ. Earth Sci.* **2016**, *75*, 1162. [CrossRef]
44. Qian, J.Z.; Xu, G.Q.; Zhao, W.D. *Groundwater Pollution Control*, 2nd ed.; Hefei University of Technology Press: Hefei, China, 2018; pp. 116–146.

45. Hayek, M. A Model for Subsurface Oil Pollutant Migration. *Transp. Porous Med.* **2017**, *120*, 373–393. [CrossRef]
46. Mateo, C.M.; Hanasaki, N.; Komori, D. Assessing the impacts of reservoir operation to floodplain inundation by combining hydrological, reservoir management, and hydrodynamic models. *Water Resour. Res.* **2014**, *50*, 7245–7266. [CrossRef]
47. Zhang, Z.H.; Qian, M.M.; Wei, S. Failure Mechanism of the Qianjiangping Slope in Three Gorges Reservoir Area, China. *Geofluids* **2018**, *2018*, 3503697. [CrossRef]
48. Piman, T.; Cochrane, T.A.; Arias, M.E.; Green, A.; Dat, N.D. Assessment of Flow Changes from Hydropower Development and Operations in Sekong, Sesan, and Srepok Rivers of the Mekong Basin. *J. Water Resour. Plan. Manag.* **2013**, *139*, 723–732. [CrossRef]
49. Marinelli, F.; Niccoli, W.L. Simple analytical equations for estimating ground water inflow to a mine pit. *Ground Water* **2000**, *38*, 311–314. [CrossRef]
50. Xiong, Y.W.; Huang, G.H.; Huang, Q.Z. Modeling solute transport in one-dimensional homogeneous and heterogeneous soil columns with continuous time random walk. *J. Contam. Hydrol.* **2006**, *86*, 163–175. [CrossRef]
51. Foster, S.; van der Gun, J. Groundwater Governance: Key challenges in applying the Global Framework for Action. *Hydrogeol. J.* **2016**, *24*, 749–752. [CrossRef]